Selective Hydrogenation of CO2 to CH3OH on Supported Cu Nanoparticles Promoted by Isolated TiIV Surface Sites on SiO2

Author(s):
Noh, Gina; Lam, Erwin; Alfke, Jan L.; Larmier, Kim; Searles, Keith; Wolf, Patrick; Copéret, Christophe

Publication date:
2019-03-07

Permanent link:
https://doi.org/10.3929/ethz-b-000375899

Originally published in:
ChemSusChem 12(5), https://doi.org/10.1002/cssc.201900134

Selective Hydrogenation of CO_2 to CH_3OH on Supported Cu Nanoparticles Promoted by Isolated Ti^{IV} Surface Sites on SiO_2

Gina Noh[1], Erwin Lam[1], Jan L. Alfke[1], Kim Larmier[1,2], Keith Searles[1], Patrick Wolf[1], and Christophe Copéret[1,*]

[1] ETH Zürich, Department of Chemistry and Applied Biosciences, Vladimir Prelog Weg 1-5, 8093 Zürich (Switzerland)

[2] Current address: IFP Energies nouvelles, Rond-Point de l'échangeur de Solaize, BP3, 69360 Solaize (France)

* E-mail: ccoperet@ethz.ch

Abstract: Small and narrowly distributed Cu nanoparticles, supported on SiO_2 decorated with isolated Ti^{IV} sites, prepared via surface organometallic chemistry, show significantly improved CO_2 hydrogenation activity and CH_3OH selectivity compared to the corresponding Cu nanoparticles supported on SiO_2. We propose that these isolated Lewis acid Ti^{IV} sites, evidenced by UV-Vis spectroscopy, stabilize surface intermediates at the interface between Cu nanoparticles and the support.

The selective hydrogenation of CO_2 to CH_3OH, together with the production of H_2 from renewable sources—e.g., intermittent excess energy generated from wind or solar power—is essential to a virtuous sustainable closed-carbon fuel cycle.[1–4] Its practice, however, is complicated by the parasitic reverse water-gas-shift (RWGS) reaction, which forms CO instead. The most prominent catalysts for selective CO_2 hydrogenation to CH_3OH are Cu-based, although their activity and CH_3OH selectivity dramatically depend on the oxide support.[5–8] Cu supported on ZrO_2 (Cu/ZrO_2, where "Cu/X" denotes Cu nanoparticles dispersed on support X) has shown promising activity and high CH_3OH selectivity compared

to Cu/SiO_2.[9–12] While SiO_2 can be considered as an inert support for the Cu nanoparticles that catalyze the reaction, ZrO_2 provides Zr^{IV} sites interfacing Cu nanoparticles that act as Lewis acid sites and promote CH_3OH synthesis.[9] In fact, Cu nanoparticles supported on SiO_2 decorated with isolated Zr^{IV} sites show CO_2 hydrogenation activity and CH_3OH selectivity nearly identical to those for Cu/ZrO_2,[13] underscoring the importance of these Lewis acid sites at the periphery of Cu nanoparticles for the selective hydrogenation of CO_2 to CH_3OH.

In contrast, Cu/TiO_2 has been observed to be a very poor CO_2 hydrogenation catalyst with low reaction rates and CH_3OH selectivity,[7,8,14] in spite of the ability of Ti^{IV} metal centers, which are noteworthy Lewis acids,[15–21] to play the same role in principle as the aforementioned Zr^{IV} surface sites present in ZrO_2. This striking difference may be due to the greater reducibility of TiO_2 compared to ZrO_2, which can lead to the formation of oxygen vacancies concomitant with the reduction of Ti^{IV} to Ti^{III} and/or to strong metal-support interactions that may lead to the coverage of Cu surface atoms by TiO_x species.[22] Recent work from our group has demonstrated the ability to mitigate the reducibility of Ga_2O_3 by dispersing Ga^{III} species on the surface of an insulating support (i.e., SiO_2).[23] We therefore reasoned that the atomic dispersal of Ti^{IV} sites at the surface of SiO_2, upon which Cu nanoparticles were then supported, could promote the selective hydrogenation of CO_2 to CH_3OH by generating isolated Lewis acid sites decoupled from the bulk properties of the native oxide. We demonstrate here that such sites can be generated via a surface organometallic chemistry (SOMC) approach[24,25] to form a material – $Cu/Ti@SiO_2$ (where "$M@SiO_2$" denotes isolated metal centers M on SiO_2) – that selectively hydrogenates CO_2 to CH_3OH. In fact, the CH_3OH formation rates and CH_3OH selectivity are greater for $Cu/Ti@SiO_2$ than those for the reported $Cu/Zr@SiO_2$ materials.[13]

The catalytic material ($Cu/Ti@SiO_2$) was prepared in two steps by SOMC (Scheme 1) as follows: first, isolated Ti^{IV} sites that are free of organic ligands were generated on SiO_2 (dehydroxylated at 973 K, 10^{-3} Pa; Supporting Information, Section S1) by grafting of a Ti^{IV}

molecular precursor, $Ti(OSi(O^tBu)_3)_3(O^iPr)$,[26] followed by thermal treatment under high vacuum (10^{-3} Pa, 773 K) (Scheme 1a; Supporting Information, Section S1; this material is denoted $Ti@SiO_2$). This process generates isolated Ti^{IV} sites (vide infra) and surface silanols, which are used to subsequently graft $[Cu(O^tBu)]_4$; treatment under H_2 (101 kPa H_2, 773 K) of the resulting material (Scheme 1b; Supporting Information, Section S1) yields supported Cu nanoparticles dispersed on $Ti@SiO_2$ (referred to as $Cu/Ti@SiO_2$).

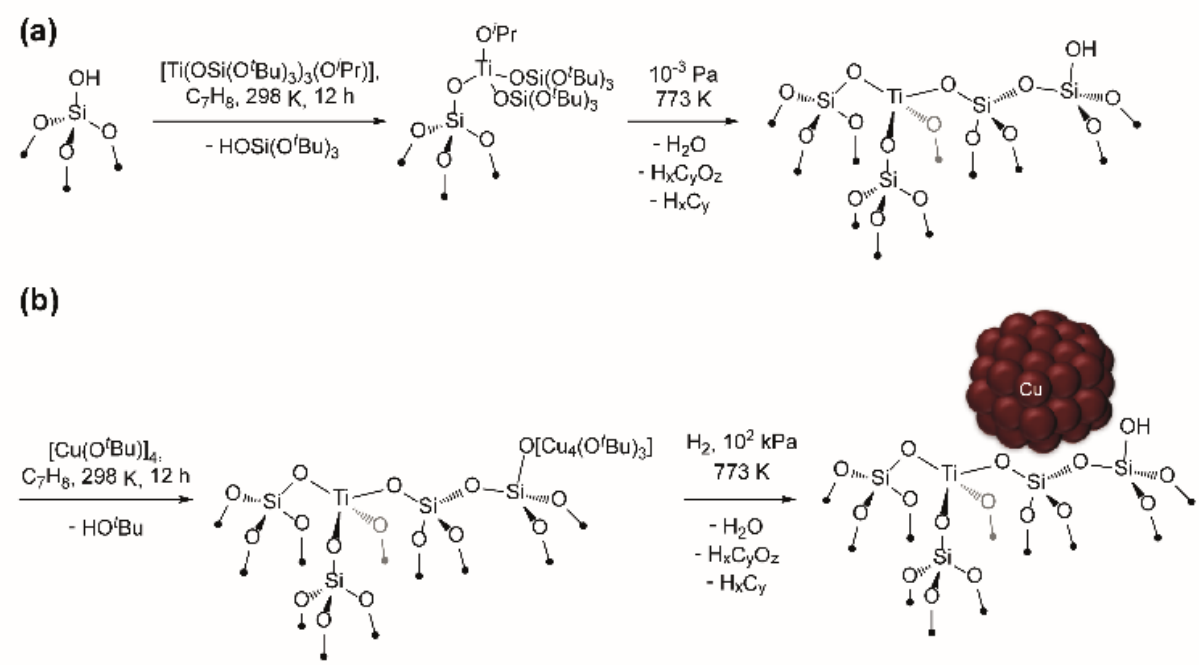

Scheme 1. SOMC approach to synthesize **(a)** $Ti@SiO_2$ and **(b)** $Cu/Ti@SiO_2$. Experimental methods and details in the Supporting Information, Section S1.

^{1}H-Nuclear magnetic resonance (NMR) spectroscopy of the supernatant used for grafting (Supporting Information, Section S1) and infrared (IR) spectroscopy of the dried solids indicate that grafting of $Ti(OSi(O^tBu)_3)_3(O^iPr)$ occurs through protonolysis and the release of one $HOSi(O^tBu)$ ligand, as evidenced by the decrease of intensity of the O-H stretching bands at 3747 cm^{-1} (Fig. 1a) and the concomitant appearance of C-H stretching (2700-3100 cm^{-1}) and bending (1300-1500 cm^{-1}) bands associated with the presence of the remaining organic ligands.

Upon thermal treatment, these C-H bands disappear while the O-H bands re-appear (Fig. 1a). This Ti@SiO_2 material contains 0.73 wt % Ti, which corresponds to an areal density of 0.45 Ti/nm^2. The isolated nature of these Ti atoms is confirmed by the narrow band at 210 nm in the diffuse reflectance UV-Vis (DRUV) spectrum (Fig. 1b), which is characteristic of the ligand-to-metal charge transfer (LMCT) from O to isolated tetrahedral Ti^{IV} centers[27,28] (spectrum for tetrahedral Ti^{IV} molecular precursor $Ti(OSi(O^tBu)_3)_3(O^iPr)$ in Supporting Information, Section S4; crystal structure included in Supporting Information, Section S2), in contrast with the features at ~390 and ~410 nm observed for TiO_2 (anatase and rutile, respectively; DRUV spectra in Supporting Information, Section S4) and the broad d-d transition band of d^1 Ti^{III} at ~700 nm (seen for the Ti^{III} molecular complex $Ti(OSi(O^tBu)_3)_3$;[29] DRUV spectrum in Supporting Information, Section S4). The absence of this d-d transition band (Fig. 1b), together with X-band electron paramagnetic resonance (EPR) spectroscopy that shows the absence of the line characteristic of Ti^{III} [g = 1.94-1.98;[30,31] spectrum in Supporting Information, Section S6 shows only a very narrow feature characteristic of C-centered radicals or free-electrons (g = 2.0023),[32] likely carbon residues formed during catalyst synthesis], indicates that the Ti@SiO_2 material contains isolated Ti^{IV} sites dispersed on SiO_2.

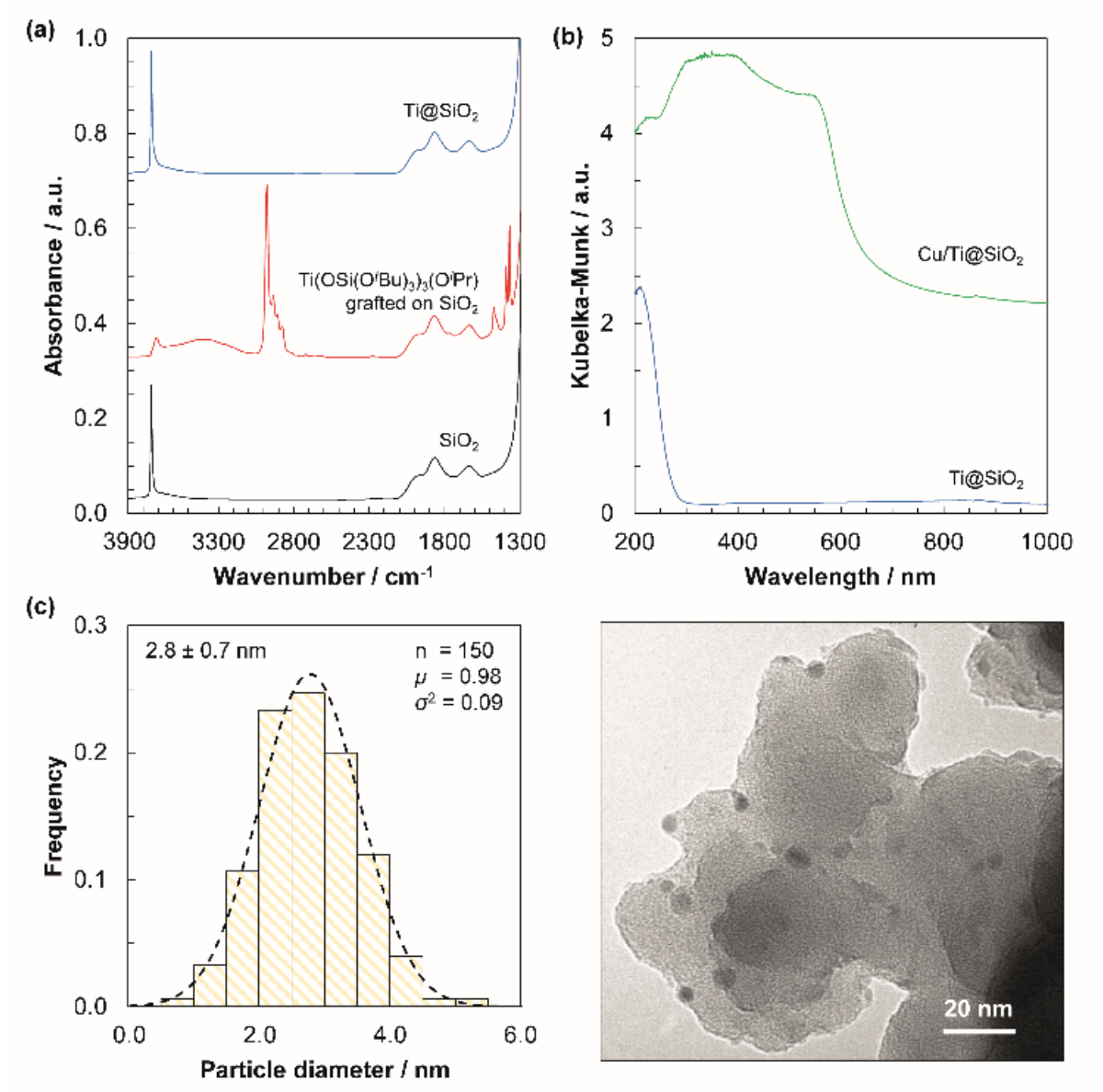

Figure 1. (a) IR spectra of (bottom) SiO_2 dehydroxylated at 973 K (discussed in the Supporting Information, Section S1), (middle) $Ti(OSi(O^tBu)_3)_3(O^iPr)$ grafted on SiO_2, and (top) isolated Ti sites decorating SiO_2 ($Ti@SiO_2$). Analogous spectra for grafting of $[Cu(O^tBu)]_4$ onto $Ti@SiO_2$ and SiO_2 are included in the Supporting Information (Section S3). **(b)** DRUV spectra of (bottom) $Ti@SiO_2$ and (top) $Cu/Ti@SiO_2$. **(c)** Histogram of Cu nanoparticle diameters (2.8 ± 0.7 nm diameter; n = 150 particles) and representative micrograph for $Cu/Ti@SiO_2$. Dashed line overlaying the histogram represents the regressed lognormal distribution ($\mu = 0.98$, $\sigma^2 = 0.09$); scale bar represents 20 nm.

Upon reaction of $[Cu(O^tBu)]_4$ with $Ti@SiO_2$, the O-H stretching bands decrease in intensity (spectra in Supporting Information, Section S3) due to grafting and reappear following treatment under H_2 (773 K) as Cu nanoparticles are generated (vide infra). The $Cu/Ti@SiO_2$ material contains 4.5 wt % and 0.7 wt% Cu and Ti, respectively, and is free of organic ligands, as indicated by the absence of the C-H stretching (2700-3100 cm^{-1}) and bending (1300-1500 cm^{-1}) bands (spectra in Supporting Information, Section S3). Transmission electron microscopy (TEM) of $Cu/Ti@SiO_2$ shows the formation of small and narrowly distributed Cu nanoparticles with 2.8 ± 0.7 nm diameter (Fig. 1c). The isolated Ti^{IV} sites retained their oxidation state after the reduction of the material to form Cu nanoparticles, as demonstrated by the absence of Ti^{III} features in the EPR spectra for $Cu/Ti@SiO_2$ (Supporting Information, Section S6). The DRUV spectrum (Fig. 1b) for $Cu/Ti@SiO_2$ shows the narrow LMCT band for O-Ti and the broad band attributed to the localized surface plasmon resonance (LSPR) for fully reduced Cu nanoparticles (520-580 nm;[33] Supporting Information, Section S4 shows DRUV spectrum for Cu/SiO_2). For comparison, Cu/SiO_2 (4.6 wt %) was prepared using the same approach (Scheme 1b; Supporting Information, Section S1; IR spectra in Supporting Information, Section S3) and also shows small and narrowly distributed Cu nanoparticles of similar size (2.8 ± 0.3 nm diameter; Supporting Information, Section S5). The nearly identical IR spectra of $Cu/Ti@SiO_2$ and Cu/SiO_2 with adsorbed CO (3.5 kPa CO, 298 K; spectra in Supporting Information, Section S7) suggest that the metal nanoparticles of both materials are composed of Cu^0. Both supported Cu materials were further characterized using N_2O frontal chromatography[34] to evaluate the number of accessible surface Cu sites (Cu_s); these similar values (Cu_s = 46 and 55 μmol.g^{-1} for $Cu/Ti@SiO_2$ and Cu/SiO_2, respectively, assuming 2:1 Cu/N_2O stoichiometry), together with similar particle size distributions from TEM, indicate that Cu nanoparticles are similar in size and in accessible surface area, irrespective of whether they are supported on $Ti@SiO_2$ or SiO_2.

With these materials in hand, we evaluated their catalytic performance in CO_2 hydrogenation. The rates and product selectivities were measured at various CO_2 residence times (0.2-12 $s.g_{Cu}.\mu mol^{-1}$; 0.5 MPa CO_2, 1.5 MPa H_2, 2.5 MPa, 503 K; Supporting Information, Section S1) for Cu/Ti@SiO_2, Ti@SiO_2, and Cu/SiO_2. Reactant conversion and products were undetectable in the reactor effluent for Ti@SiO_2, indicating that isolated Ti^{IV} metal sites alone are unable to catalyze CO_2 hydrogenation. Rates were extrapolated to zero residence time (i.e., zero reactant conversion; extrapolation discussed in Supporting Information, Section S1) to obtain initial formation rates, in order to account for the significant effects of residence time on product formation rates (Fig. 2b; vide infra) and thus to permit accurate comparison among catalysts. Initial CH_3OH formation rates (Table 1; Fig. 2a) were more than a factor of four greater for Cu/Ti@SiO_2 than for Cu/SiO_2 (18 $\mu mol.s^{-1}.g_{Cu}^{-1}$ vs. 3.6 $\mu mol.s^{-1}.g_{Cu}^{-1}$). Similarly, molar CH_3OH selectivities decreased from 85% for Cu/Ti@SiO_2 to 49% for Cu/SiO_2. In contrast, initial CO formation rates are nearly the same for Cu/Ti@SiO_2 and Cu/SiO_2 (3.1 and 3.8 $\mu mol.s^{-1}.g_{Cu}^{-1}$, respectively). Compared to previously reported initial rates for Cu/Zr@SiO_2[13] (included in Table 1), which were collected at similar reaction conditions, CO formation rates are nearly identical (3.9 $\mu mol.s^{-1}.g_{Cu}^{-1}$ for Cu/Zr@SiO_2), while CH_3OH formation rates are nearly a factor of two greater for Cu/Ti@SiO_2 than Cu/Zr@SiO_2 (18 and 10.8 $\mu mol.s^{-1}.g_{Cu}^{-1}$, respectively).

Table 1. Initial CH_3OH and CO formation rates and CH_3OH molar selectivities for supported Cu catalysts.

Catalyst	CH_3OH formation rate[a]	CO formation rate[a]	Molar CH_3OH selectivity
$Cu/Ti@SiO_2$	18	3.1	0.85
Cu/SiO_2	3.6	3.8	0.49
$Ti@SiO_2$ [b]	--	--	--
$Cu/Zr@SiO_2$ [c]	10.8	3.9	0.73

[a] units: $\mu mol.(g_{Cu}.s)^{-1}$
[b] products in reactor effluent below detection limits
[c] Ref: [13]; extrapolated to zero CO_2 residence times (Supporting Information, Section S1).

The effects of reactor residence time on CH_3OH synthesis rates and RWGS rates are also revealing. CH_3OH synthesis rates (Figure 2b) and RWGS rates (Figure 2c) for $Cu/Ti@SiO_2$ decrease dramatically with increasing residence time, while those for Cu/SiO_2 are much less sensitive to changes in residence time. Such trends for $Cu/Ti@SiO_2$ are consistent with product inhibition, whereby product H_2O or CH_3OH inhibits formation rates by competitively adsorbing to active sites at higher CO_2 conversions; nearly identical decreases in CH_3OH rates with increasing residence time were observed for Cu/ZrO_2[9] and $Cu/Zr@SiO_2$,[13] suggesting that the same pathways mediate CO_2 hydrogenation on these materials. The near absence of these residence time effects for Cu/SiO_2, a material in which Cu nanoparticles alone are responsible for conversion of the reactant and the support itself can be considered innocent, indicates that these active sites that are affected by product inhibition cannot be located solely on the Cu surface.

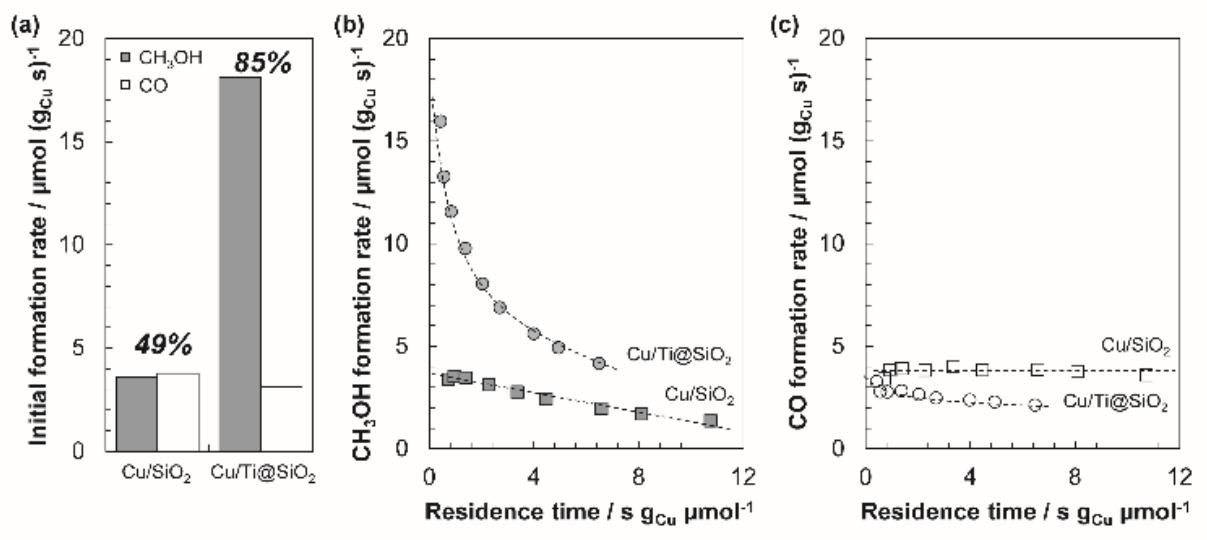

Figure 2. (a) Initial formation rates for CO (white) and CH_3OH (grey) for Cu/SiO_2, $Cu/Ti@SiO_2$, and $Cu/Zr@SiO_2$. Percentages indicate molar selectivity to CH_3OH; **(b)** CH_3OH and **(c)** CO formation rates as a function of residence time on Cu/SiO_2 (triangles) and $Cu/Ti@SiO_2$ (circles). Dashed lines represent trends. 503 K, 2.5 MPa, 0.5 MPa CO_2, 1.5 MPa H_2. Experimental details in the Supporting Information, Section S1.

The presence of residence time effects on rates for $Cu/Ti@SiO_2$ but not Cu/SiO_2 suggests that these Ti sites decorating SiO_2 play a critical role in CH_3OH synthesis. EPR spectroscopy of the $Cu/Ti@SiO_2$ catalyst following catalytic testing revealed that Ti^{IV} sites retain their oxidation state, as indicated by the absence of features indicative of Ti^{III} (Supporting Information, Section S6). These data together are consistent with the expectations based on previous conclusions of the role of Zr^{IV} sites in Cu/ZrO_2 and $Cu/Zr@SiO_2$[9,13] that Lewis acid sites at the periphery of Cu nanoparticles promote CH_3OH synthesis.

To confirm the Lewis acid nature of these isolated Ti^{IV} sites, IR spectra were collected during the desorption of pre-adsorbed pyridine – a well-known titrant for Lewis acid sites[35] – at different temperatures (details in the Supporting Information, Section S1) for $Cu/Ti@SiO_2$ and Cu/SiO_2. Vibrational bands associated with hydrogen-bonded pyridine[35] (ν = 1599 cm^{-1}

and 1447 cm^{-1}) were observed in the IR spectra for Cu/SiO_2 and $Cu/Ti@SiO_2$ (Supporting Information, Section S7). The spectra for $Cu/Ti@SiO_2$ (Supporting Information, Section S7) shows an additional band at higher frequency (ν = 1608 cm^{-1}), indicative of the coordination of pyridine to Lewis acid sites.

Ex situ solid-state NMR experiments further demonstrated the importance of such Lewis acid sites by investigating the presence and identity of surface intermediates on $Cu/Ti@SiO_2$; these surface species are similar to those observed for $Cu/Zr@SiO_2$ and Cu/ZrO_2.[9,13] The ^{1}H-^{13}C HETCOR spectrum (Figure 3) of the $Cu/Ti@SiO_2$ catalyst contacted with 5 bar of $^{13}CO_2$ and $^{1}H_2$ (in 1:3 ratio) for 12 h at 503 K (experimental details and additional solid-state NMR spectra in the Supporting Information, Section S8) shows the presence of signals assigned to methoxy (correlation peaks at $\delta(^{13}C)/\delta(^{1}H)$ = 48 ppm/2 ppm and 65 ppm/3 ppm) and formate (correlation peaks at $\delta(^{13}C)/\delta(^{1}H)$ = 170 ppm/8 ppm).[9] Such signals are not observed in the absence of Lewis acidic single sites for Cu/SiO_2[9] or in the absence of Cu nanoparticles for $Ti@SiO_2$, indicating that both these Lewis acidic single sites and Cu nanoparticles are required for their formation. We thus propose that the promotional role of Ti^{IV} in the selective hydrogenation of CO_2 to CH_3OH is the same as that of Zr^{IV}, based on similar site requirements and surface species.

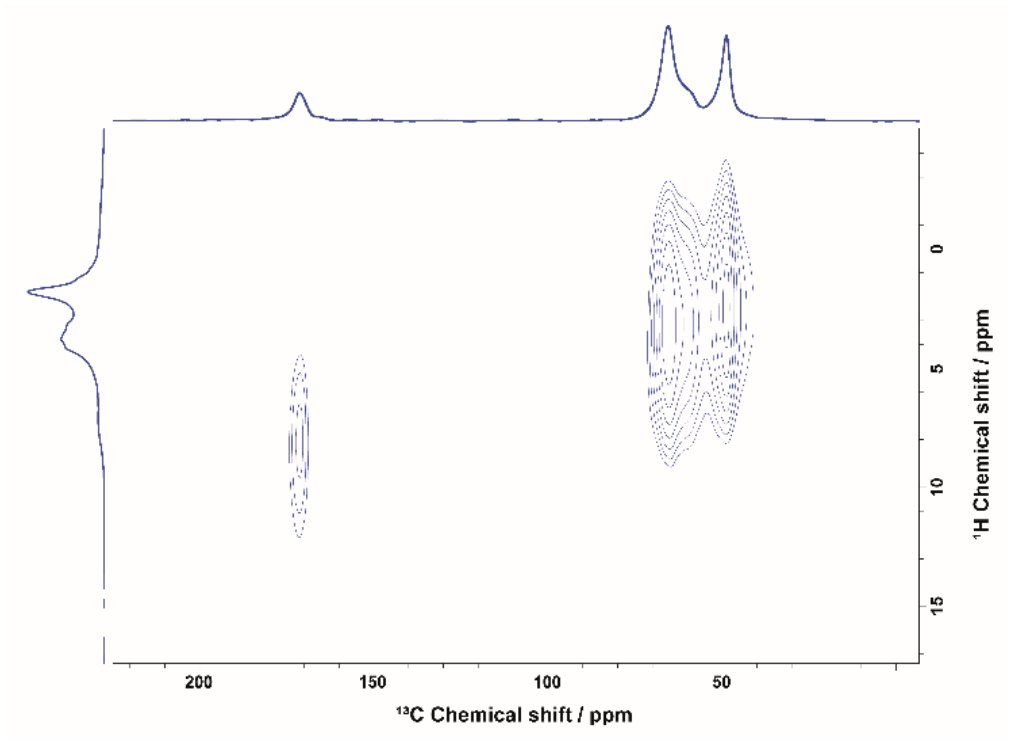

Figure 3. Ex situ ^{1}H-^{13}C HETCOR spectrum of Cu/Ti@SiO_2 after exposure to $^{13}CO_2$ and $^{1}H_2$ (1:3 ratio; 5 bar total pressure, 503 K, 12 h). Experimental details in the Supporting Information, Section S8.

We have demonstrated here the synthesis of a tailored catalyst with isolated Ti^{IV} sites on SiO_2 and dispersed Cu nanoparticles. The presence of isolated Ti^{IV} Lewis acid sites at the periphery of Cu nanoparticles promote CH_3OH synthesis. The SOMC approach used here takes advantage of the Lewis acid character of Ti^{IV} isolated metal centers on a SiO_2 surface, while avoiding the bulk properties of the parent oxide (e.g., the reducibility of TiO_2). Such an approach can be used to develop tailored supports to target characteristics of single metal sites to promote CO_2 hydrogenation and other heterogeneously catalyzed reactions.

Acknowledgments

G.N., E.L., K.L., and P.W. were supported by the SCCER—Heat and Energy Storage program. We thank C. Gordon (ETHZ) for assistance with the NMR studies; Dr. T.-H. Lin (ETHZ) for

TEM; Dr. F. Allouche (ETHZ) for assistance in the synthesis of $Ti(OSi(O^tBu)_3)_3$); and A. Ashiuev (ETHZ) for the EPR studies and helpful discussions.

CCDC 1882540 contain the supplementary crystallographic data for this paper. These data are provided free of charge by The Cambridge Crystallographic Data Centre.

Keywords: CO_2 hydrogenation • surface organometallic chemistry • CH_3OH synthesis • heterogeneous catalysis • titanium

References

[1] G. A. Olah, A. Goeppert, G. K. S. Prakash, *Beyond Oil and Gas*, Wiley-VCH Verlag GmbH & Co. KGaA, Weinheim, Germany, **2018**.

[2] A. Goeppert, M. Czaun, J.-P. Jones, G. K. Surya Prakash, G. A. Olah, *Chem. Soc. Rev.* **2014**, *43*, 7995.

[3] G. A. Olah, *Angew. Chemie Int. Ed.* **2013**, *52*, 104.

[4] G. A. Olah, A. Goeppert, G. K. S. Prakash, *J. Org. Chem.* **2009**, *74*, 487.

[5] S. Dang, H. Yang, P. Gao, H. Wang, X. Li, W. Wei, Y. Sun, *Catal. Today* **2018**, DOI 10.1016/j.cattod.2018.04.021.

[6] A. Álvarez, A. Bansode, A. Urakawa, A. V. Bavykina, T. A. Wezendonk, M. Makkee, J. Gascon, F. Kapteijn, *Chem. Rev.* **2017**, *117*, 9804.

[7] S. Kattel, B. Yan, Y. Yang, J. G. Chen, P. Liu, *J. Am. Chem. Soc.* **2016**, *138*, 12440.

[8] K. H. Lee, J. S. Lee, *Korean J. Chem. Eng.* **1995**, *12*, 460.

[9] K. Larmier, W.-C. Liao, S. Tada, E. Lam, R. Verel, A. Bansode, A. Urakawa, A. Comas-Vives, C. Copéret, *Angew. Chemie Int. Ed.* **2017**, *56*, 2318; *Angew. Chemie* **2017**, *129*, 2358.

[10] C. Schild, A. Wokaun, A. Baiker, *J. Mol. Catal.* **1990**, *63*, 223–242.

[11] J. Weigel, R. A. Koeppel, A. Baiker, A. Wokaun, *Langmuir* **1996**, *12*, 5319.

[12] I. A. Fisher, H. C. Woo, A. T. Bell, *Catal. Letters* **1997**, *44*, 11.

[13] E. Lam, K. Larmier, P. Wolf, S. Tada, O. V. Safonova, C. Copéret, *J. Am. Chem. Soc.* **2018**, *140*, 10530.

[14] C. Liu, X. Guo, Q. Guo, D. Mao, J. Yu, G. Lu, *J. Mol. Catal. A Chem.* **2016**, *425*, 86.

[15] M. P. Coles, C. G. Lugmair, K. W. Terry, T. D. Tilley, *Chem. Mater.* **2000**, *12*, 122.

[16] C. G. Lugmair, T. D. Tilley, *Z. Naturforsch* **2004**, *3*, 1540.

[17] N. E. Thornburg, S. L. Nauert, A. B. Thompson, J. M. Notestein, *ACS Catal.* **2016**, *6*, 6124.

[18] M. Boronat, A. Corma, M. Renz, P. M. Viruela, *Chem. - A Eur. J.* **2006**, *12*, 7067.

[19] B. Notari, in *Stud. Surf. Sci. Catal.*, Academic Press Inc., **1988**, pp. 413.

[20] T. Hasebe, M. Kamigaito, M. Sawamoto, *Macromolecules* **1996**, *29*, 6100.

[21] M. Kamigaito, M. Sawamoto, T. Higashimura, *Macromolecules* **1995**, *28*, 5671.

[22] S. J. Tauster, S. C. Fung, R. L. Garten, *J. Am. Chem. Soc.* **1978**, *100*, 170.

[23] K. Searles, G. Siddiqi, O. V. Safonova, C. Copéret, *Chem. Sci.* **2017**, *8*, 2661.

[24] C. Copéret, F. Allouche, K. W. Chan, M. P. Conley, M. F. Delley, A. Fedorov, I. B. Moroz, V. Mougel, M. Pucino, K. Searles, et al., *Angew. Chemie Int. Ed.* **2018**, *57*, 6398; *Angew. Chemie* **2018**, *130*, 6506.

[25] J. Camacho-Bunquin, M. S. Ferrandon, H. Sohn, A. J. Kropf, C. Yang, J. Wen, R. A. Hackler, C. Liu, G. Celik, C. L. Marshall, et al., *ACS Catal.* **2018**, 10058.

[26] G. Takahiro, K. Takayuki, A. Yoshimoto, *J. Sol-Gel Sci. Technol.* **1998**, *13*, 975.

[27] S. Bordiga, S. Coluccia, C. Lamberti, L. Marchese, A. Zecchina, F. Boscherini, F. Buffa, F. Genoni, G. Leofanti, G. Petrini, et al., *J. Phys. Chem.* **1994**, *98*, 4125.

[28] L. Marchese, T. Maschmeyer, E. Gianotti, S. Coluccia, J. M. Thomas, *J. Phys. Chem.*

B **1997**, *101*, 8836.

[29] F. Allouche, Structure – Activity Relationship in Olefin Polymerization with Well-Defined Ti(III) and Ln(II) Molecular and Surface Complexes, PhD Dissertation No. 24906. ETH Zurich, **2018**.

[30] L.-B. Xiong, J.-L. Li, B. Yang, Y. Yu, *J. Nanomater.* **2012**, *2012*, 1.

[31] R. F. Howe, M. Gratzel, *J. Phys. Chem.* **1985**, *89*, 4495.

[32] B. Dellinger, S. Lomnicki, L. Khachatryan, Z. Maskos, R. W. Hall, J. Adounkpe, C. McFerrin, H. Truong, *Proc. Combust. Inst.* **2007**, *31*, 521.

[33] A. N. Pestryakov, V. P. Petranovskii, A. Kryazhov, O. Ozhereliev, N. Pfänder, A. Knop-Gericke, *Chem. Phys. Lett.* **2004**, *385*, 173.

[34] J. W. Evans, M. S. Wainwright, A. J. Bridgewater, D. J. Young, *Appl. Catal.* **1983**, *7*, 75.

[35] E. Parry, *J. Catal.* **1963**, *2*, 371.